How to Cite:
Mohankumar, C. E., Kumar, S. V. D., Senthilkumar, S., Sornagopal, V., & Maharajan, M. S. (2022). RNN model-based classification of wireless capsule endoscopy bleeding images. *International Journal of Health Sciences*, *6*(S1), 7330–7344. https://doi.org/10.53730/ijhs.v6nS1.6910

RNN model-based classification of wireless capsule endoscopy bleeding images

Mr. C.E. Mohankumar
Assistant Professor, Department of ECE, GRT Institute of Engineering and Technology, Tiruttani

Mr. S.V. Dharani Kumar
Assistant Professor, Department of ECE, GRT Institute of Engineering and Technology, Tiruttani
Email: dharanistrikez@gmail.com

Mr. Senthilkumar. S
Associate Professor, Department of ECE, GRT Institute of Engineering and Technology, Tiruttani
Email: senthil.swamyg@gmail.com

Mr. Sornagopal V
Associate Professor, Department of ECE, GRT Institute of Engineering and Technology, Tiruttani
Email: sornagopalv@gmail.com

Maharajan M S
Assistant Professor, Department of CSE, GRT Institute of Engineering and Technology, Tiruttani
Email: maha84rajan@gmail.com

***Abstract*---**WCE (wireless capsule endoscopy) is a technique that may be used to diagnose gastrointestinal issues and provide painless gut imaging. Regardless, a variety of variables, such as effectiveness, tolerance, safety, and performance, make widespread use and modification challenging. Furthermore, automated analysis of the WCE data is essential for detecting anomalies. When a patient's digestive system is imaged using WCE, a vast amount of data is generated and these challenges have been addressed using a variety of computer assisted and vision-based technologies, but they do not achieve the essential level of precision, and further work is required. With this work, the goal is to create a system that can automatically analyze WCE images to identify problems and assist practitioners in making right diagnoses. Finally, a comparison of SODM-S1 with SODM shows that by modifying features to increase spatial

dependency, our suggested technique may really improve model performance.

***Keywords*---**Endoscopy, RNN, Machine Learning.

Introduction

Infections in the gastrointestinal system, have become more common in recent years, including ulcer polyps, bleeding and Crohn's disease, while ulcers and bleeding are common illnesses. Lung cancer is the leading cause for death (1,1 million deaths), followed by carcinogenic cancer of the United States (765 000 deaths), colon and rectum cancer (525 000 deaths), liver cancer (505 000 deaths), as well as breast cancer and breast cancer (385 000 deaths), respectively (WHO, 2020). There were 135,430 new cases of gastrointestinal tract infections reported in the United States in 2017, with an average of 200,000 new cases per year since 2011. If discovered and diagnosed early enough, this gastrointestinal tract infection may be treated (Y. Fu et.al., 2014). Experienced doctors rely on wireless capsule endoscopy to diagnose gastrointestinal tract illness.

Endoscopy using a wireless capsule is a means of imaging the small intestine that is noninvasive (M. Sharif, et.al., 2019). The patient must swallow a capsule of a camera equipped device that passes over the digestive system and shoots it before it can be transmitted to an external receiver. The WCE technology, which was first developed by a research group in 1989, has undergone many modifications throughout time by different businesses to become more precise and efficient, as it is now (R. L. Siegel et.al, 2017). Old endoscopy causes great discomfort and distress for patients, therefore this technology replaced the traditional endoscopic procedure and simplified the diagnostic process for both patient and examiner alike. During the WCE procedure, a camera within the patient takes pictures continuously for 8 hours and sends about 60000 images to the receiver (T. Rahim et.al., 2019). The physician can decide which frames / pictures have the disease using these photographs. Due to the large number of images, a medical professional must spend a significant amount of time examining them, which may add to the practitioner's workload and lead to a delayed identification of the infected intestinal area. A popular academic issue in recent years has been finding polluted areas in photos using different statistical and machine learning methods.

A large number of images are analysed automatically and those which are infected are identified. This enables the doctor to concentrate on only those images which contain visual information from the infected area and to take immediate remediation measures. Machine learning methods have shown considerable proficiency in doing such automated tasks and have the potential to progress and improve the medical sector. Many researchers are utilising artificial intelligence to develop automated methods for gastrointestinal tract infection detection (X. Liu et al., 2012) and classification (Y. Yuan et al., 2017). In their methods, the researchers mostly examine a particular illness in automated detection systems, such as ulcer (Y. Yuan, et al., 2015), polyps (J. Bernal, et al., 2015), and bleeding (Y. Yuan, et al., 2016), since it is efficient and specialised for

a specific job. In a similar vein, this research uses the machine learning paradigm to categorise gastrointestinal tract infection (bleeding) pictures.

Related Work

For the last two decades, only a small number of reviews have been conducted in the area of WCE image analysis, with an emphasis on model designs and performance. The majority of the responses to the survey are concerned with the different characteristics used to describe anomalous patterns and the classifiers used to classify them (Trasolini, R., et al. 2021, Rahim, T., et al. 2020 & Muhammad, K., et al. 2020). This article focuses on new research in WCE image analysis and medical image analysis that has just been published. Study includes general medical image analysis publications as well as deep learning models in order to gain a broader understanding of deep learning models.

In the field of image analysis, Ali, H., et al. conducted a full study of computer-aided detection approaches (2019). Various endoscopic techniques were detailed in detail, and strategies for extracting colour and texture features in the spatial, geometric, and frequency domains were examined. Furthermore, the study discusses several deep learning models that have been published for WCE image analysis, as well as provides publicly accessible datasets. Furthermore, the survey demonstrates that the literature did not consider the dataset quality, Their investigation found a dataset class imbalance or a lack of

A few research that investigated for aberrations in the WCE domain were examined by Sreekutty, K., and Hrudya, K. P. (2017) A variety of factors are taken into consideration when evaluating the product, including color, texture. The performance, benefits, and drawbacks of feature extraction techniques were also discussed.

The papers proposed for Endoscopic Computer Assisted Detection were reviewed by Liedlgruber, M., &Uhl, A. (2011). In the field of medical processing, the spatial field, frequency domain and high-level features were considered common. The survey compares SVM and k-NN classifier performance and discusses future research possibilities.

"W. Du and colleagues" (2019) studied the latest literature on anomaly identification using deep learning in various endoscopic procedures (Colonoscopy, Gastroscopy and WCE).

WCE image analysis was divided into three domains: Detection, Classification, and Segmentation. The results of the endoscopic image analysis included LeNet, AlexNet, GoogLeNet, VGGNet, ResNet, R-CNN, FCN, SegNet and DeepLab, along with their evaluations in performance. The author also stressed in conclusion the importance of the DL diagnostic system 3D-CNN, real time video processing and the development of RNN and GNN.

Proposed Method

WCE images are a time-consuming and cumbersome procedure for doctors as a single patient scan can include tens of thousands of GI images. An experienced doctor can take hours to evaluate each case. Furthermore, aberrant frames may only account for a small percentage of the total number of pictures collected (B. Li et. al., 2009). As a result of tiredness or negligence, doctors may overlook the real problem. There are improvements in ulcer identification, polyp recognition, and bleeding area segmentation that have prompted researchers to resort to computer-aided methods in order to minimise the load on doctors and ensure diagnostic accuracy.

Figure 1: Illustration of a wireless capsule

Ulcers are one of the most frequent GI tract lesions, with an estimated 1 out of every 10 people suffering from them. Ulcers are injured tissue that has a breach or discontinuity in the bodily membrane caused by stomach juices. The ulcerated region has a distinct hue and texture than the rest of the GI tract. Figure 2 depicts several typical ulcer frames from WCE videos. Each frame in the WCE video should or should not be classified as ulcerated or computer-specifically classified.

As computer vision projects (such as ImageNet and COCO) have become more complex, the rate of error increases In the last few years, several deep learning structures such as AlexNet, VGGNet, GoogLeNet and ResNet have been developed. Many investigators realised that handcrafts contain only a part of the information in WCE pictures, and that deep learning techniques may extract strong feature representations for WCE lesion identification and depth estimation.

Figure 3 depicts an overview of the bleeding detecting system. From a frame of WCE video, the three colour areas with the most information are extracted. A multi-layer perceptron (MLP) structure is used because to the restricted power capacity and other hardware limitations. The network connections are quantized for further simplicity and integrating the entire system within capsule endoscopy. The suggested system is then described in more depth in the next phase.

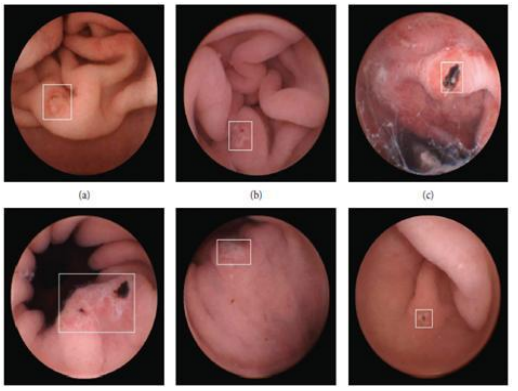

Figure 2: An ulcer as seen in a typical WCE image Each image has a white frame around the areas that are infected

Conversion of colour spaces

Colors may be represented in a variety of ways, and certain characteristics are more representative in each colour space. The green channel, for example, is more helpful than the others in retinal picture analysis. Before any medical image processing, colour space conversion may be thought of as a pre-processing step. The colour spaces in HSV and CIE are two options for RGB colour space. The CIE laboratory is user-friendly and aims to imitate the visual system of humans. Color is represented by the L, "a," and "b" components, with L ranging from 0-100 and "a" and "b" ranging from - 110 to 110. The colour area in the HSV with its colour, saturation and value is very similar to the way people see colour. Figure 2 shows a leaking frame from a WCE video in several colour spaces. As seen in Fig. 2, certain colour spaces better depict bleeding areas than others, while others provide no relevant information. A simple experiment may be used to determine whether colour schemes or channels are appropriate for representing bleeding areas. Each pixel value in each channel is regarded as a look-up table index (LUT). For bleeding areas in all pictures in the collection, the content of LUT in the associated indices is raised. It is feasible to determine the most appropriate colour space or channel by evaluating the contents of the LUT in bleeding areas. Saturation, the "a" component, and grey scale representation were chosen as the best colour characteristics in this experiment. Grayscale conversion, saturation, and the "a" channel all contain unique information regarding the bleeding area, as seen in Fig. 2.

Neural Network

The WCE image areas are classified using an MLP structure for local categorization of the bleeding regions, as shown in Fig. 2. A patch is considered around each pixel. As the MLP's input, extracted patches from three colour spaces are aligned. A patch's center pixel class is determined by a network's output during training. Two neurons are considered the network's output, and a SoftMax operation determines the final class of the input patch, similar to other binary classification issues. Because of the WCE's resource constraints, no further feature extraction or pre-processing has been performed. Experiments on

WCE pictures reveal that just 0.2 percent of pixels are in the bleeding class, with the remainder being non-bleeding, or unbalanced data. During the training phase, this issue is addressed by utilising an equal amount of bleeding and nonbleeding pixels.

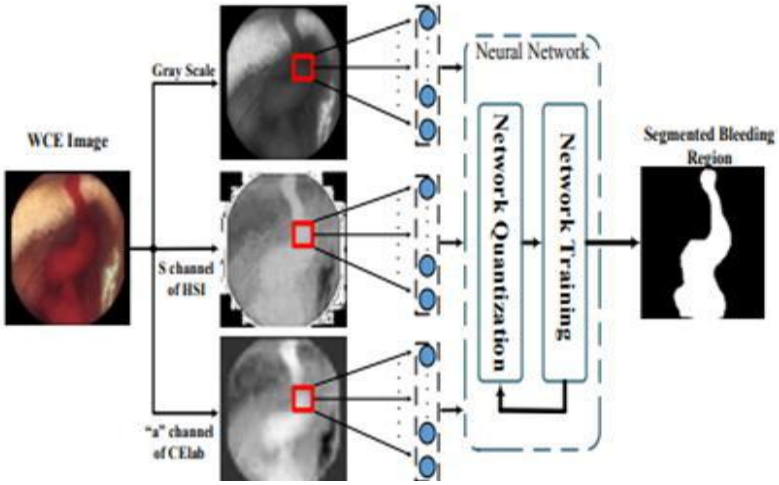

Figure 3. Overview of the proposed system

Quantification of Neural Networks

In terms of hardware implementation, an artificial neural network structure is made up of three components. Multiplication is used to create weights, addition is used to give input to the activation functions, and a non-linear activation function may be implemented as a piecewise linear function.

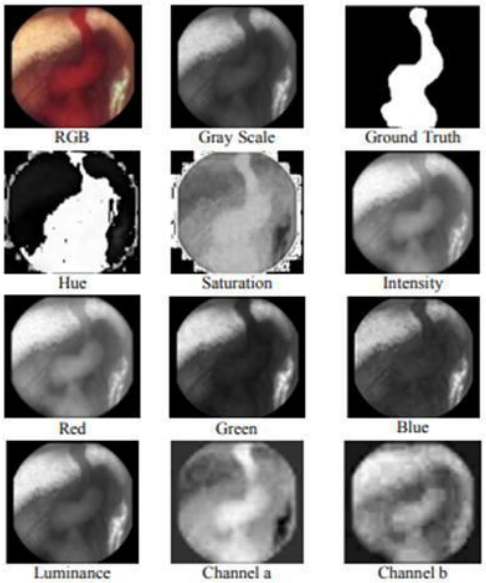

Figure 4. Different color spaces

Binarization has recently been discovered to be an effective method of reducing the complexity of network structures. All connections are subjected to network structure simplification. Binarization transforms a value to two alternative values, such as 0 and 1.Previous research [20, 21] proposed two techniques for binarization. (1) and (2) demonstrate deterministic and stochastic binarization of network weights, respectively.

$$W_b = \begin{cases} +1 & if\ W \geq 0, \\ -1 & otherwise. \end{cases}$$

$$W_b = \begin{cases} +1 & with\ probability\ p = \sigma(w), \\ -1 & with\ probability\ 1-p. \end{cases}$$

$$\sigma(x) = clip\left(\frac{x+1}{2}, 0, 1\right) = \max(0, \min(1, \frac{x+1}{2}))$$

where is network weight before quantization and is binarized one and ( ) in (3), is the „" hard sigmoid function". In this paper deterministic ternary quantization of the weights is considered as (4).

$$W_b = \begin{cases} -1 & if\ W < 0 \\ 0 & if\ W = 0 \\ 1 & if\ W > 0 \end{cases} \qquad (4)$$

The approximate power consumption of operations with various representations was given in (M. Horowitz, 2014). In compared to 32-bit format, binary representation uses 32 times less memory and requires 32 times fewer memory accesses. It is also worth noting that with fewer bit length representation of the weights, substantially reduced energy consumption and multiplication operations.

Results and Discussion

Experimental Results and Analysis

Data Preparation

In order to investigate the effectiveness of our proposed SODM for small intestinal diseases detection, Normal and aberrant elements of the datasets are taken into account.

Performance on outlier detection of small intestinal diseases

Comparison Methods

In the following table, we compare our model with a variety of outlier detection

- ResNet50 + K-nearest neighbors algorithms (KNN);
- ResNet50 + Local outlier factor (LOF) (H. Ma, Y. Hu, et. at., 2013);
- ResNet50 + One-class SVM (OC-SVM) (D. Fernández-Francos, et. al., 2013);
- ResNet50 + Support Vector Data Description (SVDD) (J. Huang et., al 2016);

- ResNet50 + One-class Conditional Random Field (OC-CRF) (Y. Song, et. al., 2016);
- Deep Structured Energy based Model (DSEBM) (S. Zhai, et. al., 2016);
- Unsupervised Outlier Detection Model (UODA) (W. Lu, et. al., 2017);
- Early Fault Detection Model (FDDA) (W. Lu., et, al., 2018);
- A simple version of SODM (SODM-S1)

One of the most used frameworks in the area of outlier identification is 1-5, which includes a feature extraction stage as well as an outlier detection stage. A pre-trained ResNet50 architecture is used as a feature extractor in Methods 1-5, which is consistent with our past work.Traditional outlier identification approaches In order to develop a discriminating model for normal data, such as KNN, LOF, OC-SVM and SVDD are also used. There are four excellent approaches for identifying outliers in sequential data. For example, OC-CRF makes use of CRF in order to learn the reliance from To solve the problem of finding outliers, DSEBM uses an energy function in its deep generative model. Similar to UODA and FDDA, our architecture consists of two parts: a feature extraction module and a system state predictor. Our model and these two, however, still have substantial discrepancies. The distinctions may be seen in two areas. To begin with, our model has a greater capability for feature extraction and sequence modelling, which can be ascribed mostly to the model structure and successful training technique. Second, OAM provides a superior solution in our model for identifying minor intestinal illnesses with high accuracy. The final technique is a simplified form of SODM which varies in terms of training from the original SODM. In particular, we construct the CFE portion of SODM-S1 with standard form losses (10) and pi produced with an additional classification layer instead of sigmoid directly (CL). The contributions of thesuggested training technique may be readily seen in this manner.

Implementation Details

A discrete dataset is fed into the method 1-4 outlier identification portions of the pre-trained Restnet50 in order to extract input features from normal data. k-nearest neighbors (KNN) splits normal features in If the sample does not fit into any of k clusters, it is considered an outlier. By experimenting with 1, 2, 4, 8, 16, 32, 64, it is possible to identify the optimal cluster number If you're using a LOF-based strategy, the outlier is identified by comparing its maximum LOF value to the input characteristics' maximum Procedures 3 and 4 use input attributes directly to create a one-class classification model. The corresponding publications [32]–[35] contain OC-CRF, DSEBM, UODA and FDDA implementation parameters. As described in Section III below, CNN-LSTM and OAM are used in our SODM. The parameter values are shown in Table 1.

Evaluation Metric

Specificity, sensitivity, and accuracy are three kinds of assessment metrics used. False positive (FP) and false negative (FN) are the metrics that are used to quantify these measures: true positive (TP), true negative (FN). TP is the number of samples required to properly identify outliers, whereas TN denotes the number of samples required to accurately find normalities. The FP and FN values are

therefore erroneously classified as the number of normalities and outliers. The formula for calculating these metrics is as follows.

Table 1
Parameters of SODM

Parameters	Value
Input size of FTL (Output size of ResNet50 part)	2048
Output size of FTL	1024
Input size of LSTM	1024
Output size of LSTM	1024
ω_1 in situation map evaluation module	0.6
ω_2 in situation map evaluation module	0.4
Threshold for normal range of δ_{C-L}	0.4
Threshold for confirming the outlier	0.5

$$Sensitivity = \frac{TP}{TP + FN} \tag{12}$$

$$Specificity = \frac{TN}{TN + FP} \tag{13}$$

$$Accuracy = \frac{TP + TN}{TP + TN + FP + FN}. \tag{14}$$

Outlier detection results on the data set

For the application step, twenty-three WCE pictures are gathered. A total of 1219 target blocks have been developed based on the annotations of physicians, consisting of 937 normal blocks and 282 outlier blocks For example, in Table 2, you can see the values for the following: Tp (transparency), Tn (transparency), FP (forwardness), and Table 2 shows that SODM has a higher TP value than other comparison strategies. It will result in a low incidence of missed diagnoses, which is the most essential criterion for medical diagnosis. Three assessment metrics are presented in Fig. 5 for a comprehensive and in-depth examination of our approach.

The accuracy index reflects a model's overall performance; our model's accuracy is 93.27 percent, which is greater than others. Without addressing the input data correlation (Methods 1-4), KNN achieves the highest accuracy performance of 90.40 percent, which is 2.87 percent less than our model. FDDA, with 91.30 percent accuracy, is the most accurate method using sequential data analysis methodology (Method 5-9), however our model's accuracy is still 1.97 percent better. In addition, Fig. 5 has three more facts worth noting.

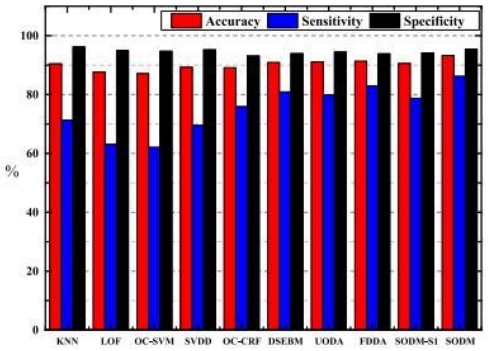

Figure 5. Variables with high levels of precision, sensitivity, and specific

To begin with, our model's performance is not much better than that of other approaches based only on accuracy (red bar) and specificity (green bar) (black bar). The composition of the dataset for application may explain why this scenario exists. The regular blocks make up the majority, accounting for 76.9% of the total. While accuracy is a measure of the model's ability to recognize normal blocks, specificity is a measure of the model's ability to identify It has a high level of accuracy and specificity, even when it is unable to filter outliers adequately, because it groups outliers into the typical category. A KNN model, for instance, is only sensitive to 71,28%, but has 90,40% and 96,160% accuracy and specificity, respectively. Sensitivity thus becomes a more meaningful measure for model performance evaluation, since sensitivity is a measure of the model's ability to In comparison to other approaches, SODM has approximately 86.17 percent sensitivity (the second highest sensitivity is 82.98 percent of FDDA). The sensitivity number indicates that SODM has a strong capacity to identify outliers. Secondly, the precise and sensitive indices of approaches 5-10 are often greater when dealing with outer identification problems than those of methods 1-4, illustrating the benefits of taking the correlation of data into account in dealing.

Figure 6 shows that CFE (blue) and LSE (black) SODM loss curves and LSE (red) SODM-S1 loss curves have been shown to help investigate this problem. The following are some of the conclusions that may be drawn: 1) Initial phases of the training process show that the black line's downward trend is smoother than any other line's (epoch 1 to 10). It's because CFE is looking for the best parameters at this point (blue line is rapidly descending), the quality of features used as input to LSE modules is impacted. This phenomenon may be seen in the variation trends between epoch 10 and 20 of the black and blue lines. In addition, because the CFE section of SODM-S1 was completed before it was incorporated into LSE, the loss curve shows a downward trend. As a result of our training technique, SODM-LSE generates a superior learning outcome compared to SODM-S1 (the black curve is lower than that of SODM-S1).

Table 2
TP, TN, FP, FN as well as accuracy, sensitivity and specificity calculated values by using various methods

ID	Method	TP	TN	FP	FN	Accuracy (%)	Sensitivity (%)	Specificity (%)
1	KNN	201	901	36	81	90.40	71.28	96.16
2	LOF	178	890	47	104	87.61	63.12	94.98
3	OC-SVM	175	887	50	107	87.12	62.06	94.66
4	SVDD	196	892	45	86	89.25	69.50	95.20
5	OC-CRF	214	872	65	68	89.09	75.89	93.06
6	DSEBM	228	880	57	54	90.89	80.85	93.92
7	UODA	225	885	52	57	91.06	79.79	94.45
8	FDDA	234	879	58	48	91.30	82.98	93.81
9	SODM-S1	222	882	55	60	90.57	78.72	94.13
10	SODM	243	894	43	39	93.27	86.17	95.41

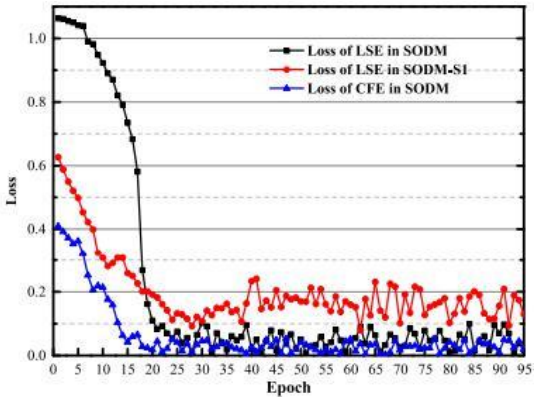

Figure 6. Loss curves of SODM and SODM-S1

ROC curves of different models

One of the most important steps in evaluating a model's practise is the receiver operating characteristic (ROC) curve. KNN and FDDA are the optimum models for various input types according to the findings of Section IV-B-4. As a consequence, we will create SODM, KNN, and FDDA ROC curves in this section for future study. The actual results are presented in Figure 8. The y-axis is composed of False Positive Rate, whilst the x-axi (f-axi) is composed of True Positive Rate (TPR), calculated using the FPR formulation = FP/(FP + TN). Furthermore, by examining the curves presented, it can be inferred that SODM is more sensitive to the presence of outliers.

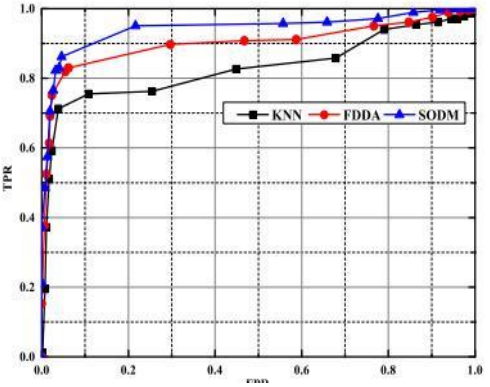

Figure 7. ROC curves of KNN, FDDA and SODM

In Figure 8 for these three models, the ROC calculation technique may be summarised as follows: outlier indications the results of the comparison are used to classify the samples. The variance value between actual input and predicted state is the indication for SODM and FDDA, when it comes to KNN, though, it's based on distance between inputs to sum up, a higher number suggests a larger chance of an outlier. The quality of indicators seems to have a direct impact on the ROC curve's performance. Therefore, only if the indicator has an outline sensitivity and a high indicator value, TPR can maintain a suitable level. The SODM TPR is superior to two other models, in order to demonstrate the sensitiveness of SODM in dealing with outside inputs (blue curve is above red and black curves).

Figure 8. Image to illustrate the process of creating outliers. Annotated red dashed circle on WCE image with ulcer. (a) Outlier Detector's candidate outlier blocks.

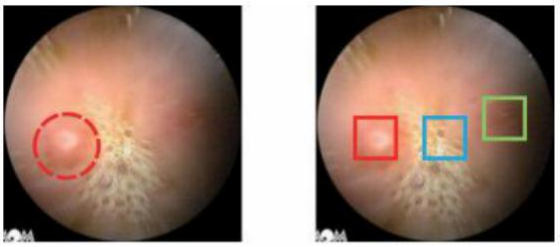

TABLE 3. Similarity degree of three candidate blocks.

Red block	Blue block	Green block
0.128	0.209	0.892

Empirical analysis

We'll talk about SODM's outlier creation method in this part. As an example, a typical picture of tiny intestinal ulcers is used. Figure 8 shows the selected picture with physicians' annotations (a). The red dashed circle surrounds the ulcer-infected region. The Outlier Detector, for starters, outputs blocks with a CL higher than the usual threshold. It would filter out blocks that are extremely similar, because the lesion area covers many blocks and each target block is examined in all respects. Representative blocks from each potential block cluster are chosen for the sake of the study. Figure 8 shows the red, blue and green sample blocks in three colours (b). Clearly, the red block identifies the outlier correctly.

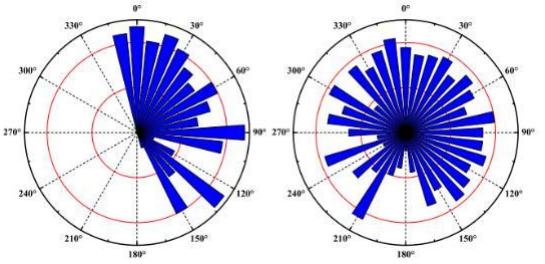

Figure 9. Block-by-block situational map Red color for the target block. Blue color for the target block

Once these three blocks have been obtained, the False Outlier Elimination Module can then use them to calculate the degree of similarity between each element in the false outlier knowledge base. Table 3 lists the blocks with the highest degree of similarity. This article states that if the similarity degree is greater than 0.7, the block is considered a false outlier. The green block will be removed from this session as a result. Final decision is made by the Situation Map Evaluation Module, which takes into account the surrounding information of the target block. The deviation values produced by sequence data are shown using a polar diagram from all directions. Figure 10 depicts the details. This is a picture of a target block on the left, and a scenario map for that block on the right, both in red FIGURE 10: The blue bar pointing in various directions reflects a calculated value of CL from the relevant direction. The smaller red circle's radius reflects the normal range's threshold, while the larger red circle's radius represents the abnormally high CL range'. However, because there isn't enough capacity on the scenario map for generating sequential data in the 170 to 340 degree zone, deviation values are missing in this zone. Three conclusions can be drawn from the study of CL bars formed from -20 degrees to 160 degrees: In Rule II, the majority of the CL values are above the normal range barrier (they surpass the smaller circle). In this way, may be computed, yielding a value of 0.69. There are seven cases where the threshold has been exceeded (the red circle is too large), which is the circumstance described in Rule III. AH has a result of 0.39. This leads to a CL with very small values occurring in the zone from 100 degrees to 110 degrees and 160 degrees. Scoreoutlier = 1 + 2 AH = 0.6 0.69 + 0.39 = 0.57 >Outlier Threshold) can assist us appropriately classify the target block into the outlier category.Despite the fact that component 3) has little effect on the end

result, it is nevertheless worth paying attention to when building a more robust model to prevent this kind of disruption. Two points should be noted about the scenario map on the right part.As a result of this, even when values of CL match the limits proposed in Rules II and III, we still eliminate the possibility of outliers with a total evaluation (Scoreoutlier = ω1 ∗μδ +ω2 ∗AHδ = 0.6∗0.61+0.4∗0.06 = 0.39 <OutlierThreshold). On the other hand, the direction of bubble areas has tiny values of CL (170 degree to 200 degree).The first instructs us on how to properly identify blue target blocks. It demonstrates that functional modules may be utilised to deal with difficult circumstances. The second point shows our model's capacity to detect spatial correlation.

Conclusion

A study using deep models for identifying abnormalities in WCE pictures was conducted. This paper examines the need to use deep models for image analysis by WCE, as well as its advantages and disadvantages. Existing profound learning models have been monitored and only require a small number of etiquetted information for Due to class imbalances, training data quality is found to be low. Semi-monitored deep learning model overcomes the problem of insufficient labelled datasets through the use of non-labeling model training data and improves overall classification accuracy by comparing supervised models previously. Semi-supervised deep models could incorporate domain information to help make decisions and a focus mechanism to learn target-specific knowledge could be used. A model for decision-tab support also helps to understand model behaviour, and according to the authors, increases the interpretability of the model.

References

P. Sivakumar1 · B. MuthuKumar, “A novel method to detect bleeding frame and region in wireless capsule endoscopy video”, 2017

R. L. Siegel, K. D. Miller, S. A. Fedewa, D. J. Ahnen, R. G. S. Meester,A.Barzi, and A. Jemal, ``Colorectal cancer statistics, 2017,''*CA, CancerJ. Clinicians*, vol. 67, no. 3, pp. 177_193, May 2017.

Y. Fu, W. Zhang, M. Mandal, and M. Q.-H. Meng, ``Computer-aidedbleeding detection in WCE video,''*IEEE J. Biomed. Health Informat.*,vol. 18, no. 2, pp. 636_642, Mar. 2014.

M. Sharif, M. A. Khan, M. Rashid, M. Yasmin, F. Afza, and U. J. Tanik,``Deep CNN and geometric features-based gastrointestinal tract diseasesdetection and classificationfrom wireless capsule endoscopy images,''*J. Exp. Theor. Artif. Intell.*,pp. 1_23, Feb. 2019.

T. Rahim, M. A. Usman, and S. Y. Shin, ``A survey on contemporarycomputer-aided tumor, polyp, and ulcer detection methods in wireless capsuleendoscopy imaging,'' 2019, arXiv:1910.00265

X. Liu, J. Gu, Y. Xie, J. Xiong, and W. Qin, ``A new approach to detectingulcer and bleeding in wireless capsule endoscopy images,'' *in Proc. IEEE-EMBS Int. Conf. Biomed. Health Informat.*, Jan. 2012, pp. 737_740.

Y. Yuan, B. Li, and M. Q.-H. Meng, ``WCE abnormality detection basedon saliency and adaptive locality-constrained linear coding,''*IEEE Trans.Autom. Sci. Eng.*, vol. 14, no. 1, pp. 149_159, Jan. 2017.

Y. Yuan, J. Wang, B. Li, and M. Q.-H. Meng, ``Saliency based ulcerdetection for wireless capsule endoscopy diagnosis,''*IEEE Trans. Med.Imag.*, vol. 34, no. 10, pp. 2046_2057, Oct. 2015.

J. Bernal, F. J. Sánchez, G. Fernández-Esparrach, D. Gil, C. Rodríguez,and F. Vilariño, ``WM-DOVA maps for accurate polyp highlighting incolonoscopy: Validation vs. saliency maps from physicians,''*Comput.Med. Imag. Graph.*, vol. 43, pp. 99_111, Jul. 2015.

Y. Yuan, B. Li, and M. Q.-H. Meng, ``Bleeding frame and region detectionin the wireless capsule endoscopy video,''*IEEE J. Biomed. Health Informat.*, vol. 20, no. 2, pp. 624_630, Mar. 2016.

M. Horowitz. “computing's energy problem and what we can do about it”, IEEE International Conference on Solid-State Circuits Digest of Technical Papers (ISSCC), pp. 10-14, 2014.

B. Li and M. Q.-H. Meng, “Computer aided detection ofbleeding regions for capsule endoscopy images,” *IEEETransactions on Biomedical Engineering*, vol. 56, no. 4,pp. 1032–1039, 2009.

H. Ma, Y. Hu, and H. Shi, „„Fault detection and identification based on the neighbourhood standardized local outlier factor method,"" *Ind. Eng. Chem. Res.*, vol. 52, no. 6, pp. 2389–2402, Feb. 2013.

D. Fernández-Francos, D. Martínez-Rego, O. Fontenla-Romero, and A. Alonso-Betanzos, „„Automatic bearing fault diagnosis based on one class ν-SVM,"" *Comput. Ind. Eng.,* vol. 64, no. 1, pp. 357–365, Jan. 2013.

J. Huang and X. Yan, „„Related and independent variable fault detection based on KPCA and SVDD,"" *J. Process Control,* vol. 39, pp. 88–99, Mar. 2016.

Y. Song, Z. Wen, C.-Y. Lin, and R. Davis, „„One-class conditional random fields for sequential anomaly detection,"" *in Proc. 23rd Int. Joint Conf. Artif. Intell.,* 2013, pp. 1685–1691.

S. Zhai, Y. Cheng, W. Lu, and Z. Zhang, „„Deep structured energy-based models for anomaly detection,"" *in Proc. 33nd Int. Conf. Mach. Learn. (ICML),* New York City, NY, USA, 2016, pp. 1100–1109.

W. Lu, Y. Cheng, C. Xiao, S. Chang, S. Huang, B. Liang, and T. Huang, „„Unsupervised sequential outlier detection with deep architectures,"" *IEEE Trans. Image Process.,* vol. 26, no. 9, pp. 4321–4330, Sep. 2017.

W. Lu, Y. Li, Y. Cheng, D. Meng, B. Liang, and P. Zhou, „„Early fault detection approach with deep architectures,"" *IEEE Trans. Instrum. Meas.,* vol. 67, no. 7, pp. 1679–1689, Jul. 2018.

WHO. (2020). Death Rate Bec